ACS Chemical Neuroscience
Cite This: ACS Chem. Neurosci. 2018, 9, 2959−2971
Research Article
pubs.acs.org/chemneuro

Stabilization and Characterization of Cytotoxic Aβ_{40} Oligomers Isolated from an Aggregation Reaction in the Presence of Zinc Ions

Benedetta Mannini,[†] Johnny Habchi,[†] Sean Chia,[†] Francesco S. Ruggeri,[†] Michele Perni,[†] Tuomas P. J. Knowles,[†,‡] Christopher M. Dobson,[†] and Michele Vendruscolo[†,*]

[†]Centre for Misfolding Diseases, Department of Chemistry, University of Cambridge, Cambridge CB2 1EW, UK
[‡]Cavendish Laboratory, Department of Physics, University of Cambridge, Cambridge CB3 0HE, UK

Supporting Information

ABSTRACT: Small oligomers formed during the aggregation of certain peptides and proteins are highly cytotoxic in numerous neurodegenerative disorders. Because of their transient nature and conformational heterogeneity, however, the structural and biological features of these oligomers are still poorly understood. Here, we describe a method of generating stable oligomers formed by the Alzheimer's Aβ_{40} peptide by carrying out an aggregation reaction in the presence of zinc ions. The resulting oligomers are amenable to detailed biophysical and biological characterization, which reveals a homogeneous population with small size, high cross-β sheet structure content, and extended hydrophobic surface patches. We also show that these oligomers decrease the viability of neuroblastoma cells and impair the motility of *C. elegans*. The availability of these oligomers offers novel opportunities for studying the mechanisms of Aβ_{40} toxicity *in vitro* and in cellular and animal models of Alzheimer's disease.

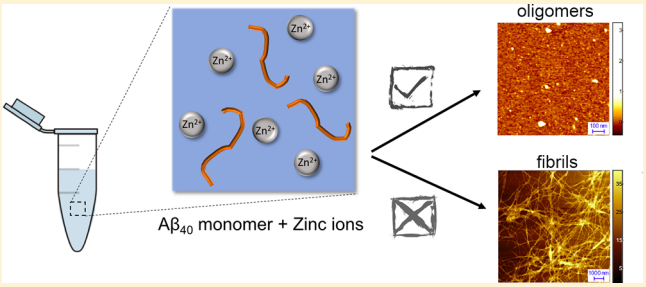

KEYWORDS: *Protein oligomer aggregates, Alzheimer's disease, antiparallel oligomer, OC-positive aggregates, amyloid, metal ions*

INTRODUCTION

Over 40 human pathologies, including Alzheimer's disease (AD), Parkinson's disease, and type 2 diabetes, have been associated with the conversion and deposition of soluble peptides and proteins into highly organized amyloid fibrils.[1−3] Irrespective of the amino acidic sequence and native structure of the aggregating polypeptide chain involved in the disease, the final fibrillar aggregates share the same inner cross-β structure: a core architecture in which an array of β-sheets runs parallel to the fibril axis, with their component β-strands perpendicular to the axis.[2−4] It has been recognized that a common mechanism underlies the fibril formation process, with an initial misfolding event followed by the self-assembly of the polypeptide chain into soluble oligomeric intermediates and, then, into insoluble fibrils.[1−3,5] It has also been established that oligomeric intermediates populate the different steps of the aggregation process: oligomers can form early during the aggregation process as on-pathway species, intermediates leading to fibril formation, or off-pathways species, end products in the process of protein aggregation unable to convert into mature fibrils, or they can be released directly by mature fibrils.[1,6,7] The oligomeric intermediates have been increasingly studied over the last two decades because they are widely thought to be the pathogenic species leading to cellular dysfunction.[8−13] However, the generally transient nature of these oligomers makes it particularly difficult to trap defined species and structurally characterize them, resulting in a gap between the atomic level resolution information currently available about fibrils and the sparse information about oligomeric species.

A number of approaches have been developed to study the structures of oligomers, allowing the identification of features shared between oligomeric species formed by different peptides or proteins.[6,14] These molecular properties are observed to vary while aggregation proceeds: initially disordered species convert into more ordered aggregates stabilized by β-sheet structure and increase their size and compactness, while hydrophobicity and flexibility decrease.[6] The aggregation process therefore seems to generate ensembles of metastable and heterogeneous oligomers, which accumulate and undergo structural rearrangements. Therefore, not only the transient formation but also the inherent polydispersity of these species constitute key technical obstacles to their investigation, resulting in major challenges in the determination of the structural elements of the oligomers that are responsible for cellular dysfunction.

Methods aimed at controlling the oligomeric stability and heterogeneity have been introduced to obtain structural models and relate the chemical and physical features to toxicity. In particular, oligomers formed by the Aβ peptide have been the subject of much attention as this peptide is the main component of the amyloid deposits found in the brain of AD patients.[1]

Received: March 26, 2018
Accepted: July 9, 2018
Published: July 9, 2018

DOI: 10.1021/acschemneuro.8b00141
ACS Chem. Neurosci. 2018, 9, 2959−2971

To stabilize Aβ oligomers different methods have been used, such as binding to small molecules,[15] photochemical cross-linking[16] and protein engineering.[17] In this study, we aimed at employing non-invasive methods and have used zinc ions (Zn^{2+}), which are normally present in the brain, to stabilize oligomers from the 40-residue form of Aβ (Aβ_{40}). This peptide, together with the 42-residue form (Aβ_{42}), is the most abundant species produced by the cleavage of the amyloid precursor protein (APP) carried out by the proteolytic enzymes β- and γ-secretase.[1,18] The two variants differ in length and aggregation propensity, but they can form similar types of oligomers, which can cause comparable cell impairment when added to cultured cells.[19]

The role of Zn^{2+} in AD has long been studied as metal ions coaggregate with Aβ and have been reported to be enriched in the amyloid plaques extracted from brain tissue of AD patients.[20−22] Because Zn^{2+} is normally present in the brain and is released at high concentrations at the presynaptic terminals of specific types of neurons,[23] the conditions under which the aggregates described in this work are obtained may mimic certain *in vivo* environments, making the Aβ_{40} oligomers that we report potentially representative of at least some forms of naturally occurring species.

Increasing evidence shows that the presence of Zn^{2+} can delay the conversion of Aβ_{40} into fibrils,[24,25] but also rapidly can promote Aβ_{40} aggregation to oligomeric species.[22,26] This phenomenon is likely to arise from the redirection of Aβ_{40} aggregation as a result of intermediate species becoming kinetically trapped and no longer being capable of forming fibrils. These effects are consistent with the stabilization of intermediate species on the aggregation pathway that culminates in amyloid fibrils. Furthermore, molecular dynamics simulations indicate that in the case of Aβ_{42}, a range of potential amyloid-like oligomers complexed with Zn^{2+} are structurally stable and could exist under appropriate conditions.[27]

We describe in this paper a method for the generation of stable and homogeneous oligomers of Aβ_{40}. By detailed biophysical investigations, we reveal that the resulting Aβ_{40} oligomers are relatively homogeneous and have the morphology, secondary structure, reactivity to conformation-specific antibodies, and tinctorial properties typical of many of the oligomers that have been described in the literature.[6] We also show that these Aβ_{40} oligomers can cause cellular dysfunction when they are exogenously added to neuroblastoma cell cultures and can decrease the motility of *Caenorhabditis elegans* worms. We thus conclude that these oligomers provide a well-defined model system with which to perform systematic and reproducible measurements using a wide range of biophysical tools and study the molecular and structural properties of toxic species related to AD to understand further the molecular basis of the toxicity associated with Aβ aggregation.

RESULTS AND DISCUSSION

A Method of Generating Aβ_{40} Oligomers. We exploited the observation that the aggregation process of Aβ_{40} is strongly dependent on the experimental conditions, including the concentration of the peptide, the pH, the ionic strength, the time of incubation, the temperature, and, in this case in particular, the concentration of Zn^{2+}. We screened a wide variety of different conditions and optimized a protocol for the formation of a population of homogeneous and stable oligomers. This protocol, summarized in Figure 1, involves several steps that can be grouped into three main procedures: (i) the expression and purification of Aβ_{40} peptide; (ii) the preparation of monomeric Aβ_{40}; and (iii) the incubation of Aβ_{40} in the presence of Zn^{2+} and subsequent isolation of the oligomers by centrifugation and resuspension.

We validated by means of thioflavin T (ThT) kinetics and SDS-PAGE (Figure S1A-D, see Supporting Information) that Zn^{2+} inhibits fibril formation by Aβ_{40} and promotes its conversion into aggregated intermediate species, as previously reported in literature.[22,24−26] Indeed, the half-time reaction, $t_{1/2}$, i.e. the time required for 50% of monomers to convert into fibrils, increased progressively as a function of the concentration of Zn^{2+} (Figure S1B). In addition, the maximum amplitude (the intensity of ThT fluorescence at the plateau of the kinetics), that reflects the amount of species able to bind to the ThT dye that are formed at the end of the reaction, decreased with the increment of the concentration of Zn^{2+} (Figure S1C). Conversely, the fraction of aggregated peptide was found to increase with the increase in the concentration of Zn^{2+}, as shown by the SDS-PAGE in Figure S1D. Taken together, these data indicate that Zn^{2+} inhibits fibril formation and concomitantly promotes the aggregation of Aβ_{40} into oligomeric species.

In our protocol, highly purified monomeric Aβ_{40} was incubated in the presence of 2:1 molar excess of Zn^{2+} at low temperature (20 °C) for 20 h. This time, based on ThT kinetic data, is sufficient to reach the plateau region of the aggregation reaction where no further evolution of the species could be detected (Figure S2A). In addition, the centrifugation step was found to be crucial for isolating and enriching the oligomeric fraction, as it enables monomeric species to be removed. Notably, an SDS-PAGE analysis revealed that the majority (∼85%) of peptide molecules had been assembled into these oligomers (Figure S2B).

Zn^{2+} Directs the Aβ_{40} Aggregation Process towards the Formation of Spheroidal, OC-Positive Aggregates. We next shed light on the stabilizing action of Zn^{2+} and the process of formation of the oligomers using high-resolution atomic force microscopy (AFM). In particular, we established non-conventional standardized experimental scanning conditions where we could maintain a constant regime of interaction between the AFM probe and the sample. This method enabled us to compare quantitatively and consistently the process of aggregation in the presence and absence of Zn^{2+} by single aggregate statistical analysis.

A time-course experiment was performed by acquiring 3D AFM morphology maps of aliquots taken from the aggregation mixture in the absence (Figure 2A) and presence of Zn^{2+} (Figure 2B) at different time points (20 min, 2, 4, 6, and 20 h). A detailed statistical analysis of the individual aggregates observed in the AFM maps was performed to quantify the distribution of the cross-sectional dimensions of the aggregated species formed during the reactions (Figure 2C). We reported the height *versus* the length of the cross-section intersecting the main axis of symmetry of the aggregates. In the case of cylindrical objects (e.g., fibrillar aggregates), the height corresponds to the diameter of their circular section perpendicular to the main axis; whereas, in the case of spheroidal objects (e.g., oligomers), the height and the length correspond simply to the diameter of the sphere. Each point in Figure 2C indicated in red or green corresponds to a single aggregate in the AFM map resulting from the incubation of Aβ_{40} in the absence or presence of Zn^{2+}, respectively.

In the absence of Zn^{2+}, the majority of Aβ_{40} molecules converts into mature fibrillar structures after 20 h of incubation

DOI: 10.1021/acschemneuro.8b00141
ACS Chem. Neurosci. 2018, 9, 2959−2971

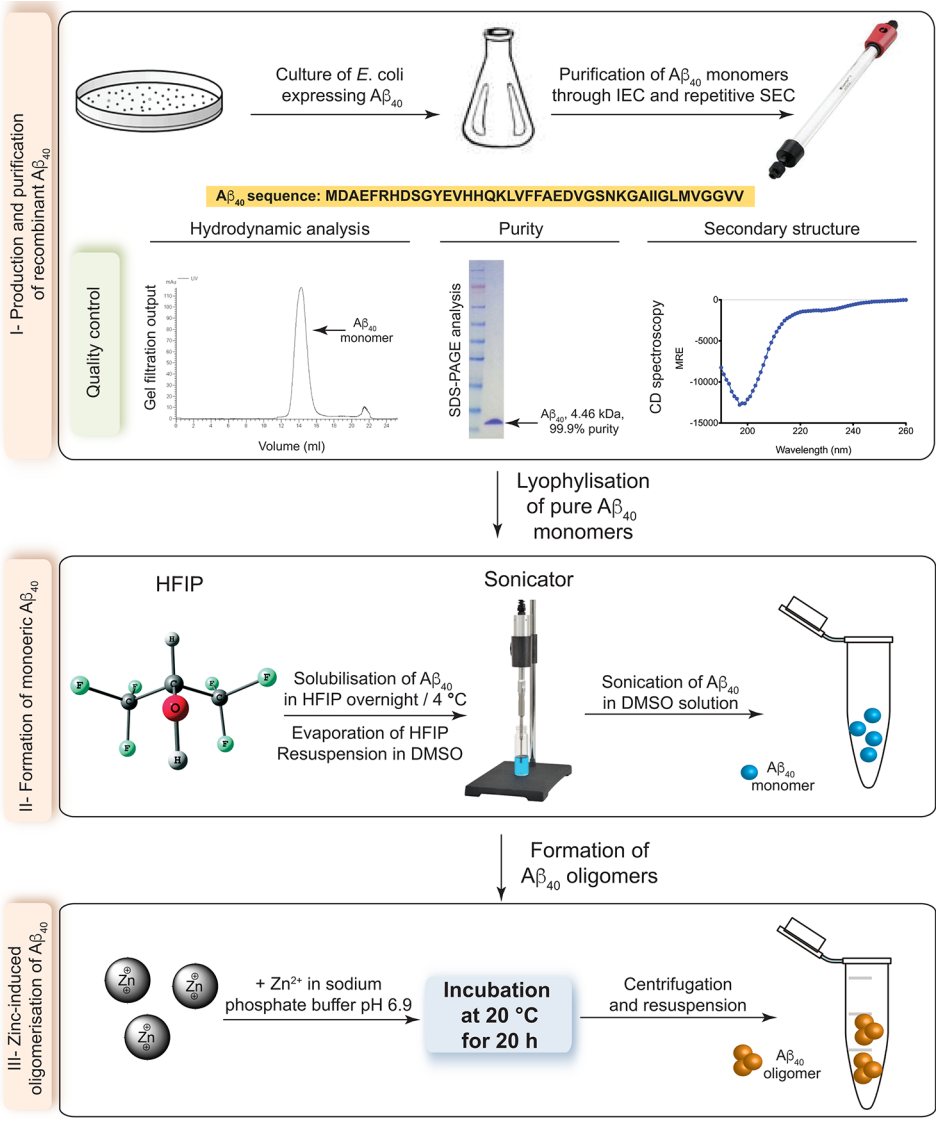

Figure 1. Schematic illustration of the procedure adopted to generate stable Aβ_{40} oligomers. The procedure can be summarized in three steps: (i) production of the Aβ_{40} peptide; (ii) formation of monomeric Aβ_{40}; and (iii) incubation of Aβ_{40} with Zn^{2+} and isolation of the oligomers by centrifugation and resuspension.

(Figure 2A). These aggregates are characterized by cross-sectional dimensions corresponding to a height of about 6 nm, which is the generally accepted AFM threshold height of an amyloid fibril having a mature cross-β sheet structure,[28,29] and a length that increases as a function of time to reach hundreds of nanometers. Aggregates with these dimensions are localized in the lower part of the length−height plots of Figure 2C. In the presence of Zn^{2+}, however, the aggregates appear to be nonfibrillar, and instead spheroidal (Figure 2B). Initially, after 20 min of incubation, the aggregates observed are either spheroidal or short chain-shaped. The spheroidal aggregates have similar heights and lengths lower than 5 nm; the short-chain aggregates have an average height of approximately 5 nm and a variable length ranging from 10 nm to more than 100 nm (Figure 2B). After 2 h of incubation, the chain-like aggregates do not appear to increase in length; instead, bigger spheroidal aggregates begin to form (Figure 2B). The presence of large spheroidal aggregates becomes more evident after 4 h of incubation. These aggregates have similar heights and lengths, reaching up to 75 nm (Figure 2B). After 6 h of incubation, the large spheroidal aggregates were more abundant and visible, and after 20 h, the majority of the visible aggregated species were spherical with diameters of up to 100 nm (Figure 2B). This population in the height-length plot at 20 h in Figure 2C occupies the plot diagonal. This AFM analysis therefore suggests that in the presence of Zn^{2+} the aggregation pathway of Aβ_{40} is directed toward the formation of spherical aggregates rather than mature fibrils under the protocol developed in this study.

The time course of the aggregation of Aβ_{40} in the presence and absence of Zn^{2+} was also investigated by means of the conformation-dependent antibodies OC and A11. These antibodies represent a useful tool because they allow recognition of distinct aggregation states of oligomeric structures, which are indistinguishable by size. Indeed, the size distributions of the oligomers recognized by the two antibodies broadly overlap, indicating the existence of distinct oligomeric conformations of the same size.[30,31] The OC antibody binds also to mature fibrils, highlighting that there is a generic epitope common to fibrils and some types of oligomers.[31]

DOI: 10.1021/acschemneuro.8b00141
ACS Chem. Neurosci. 2018, 9, 2959−2971

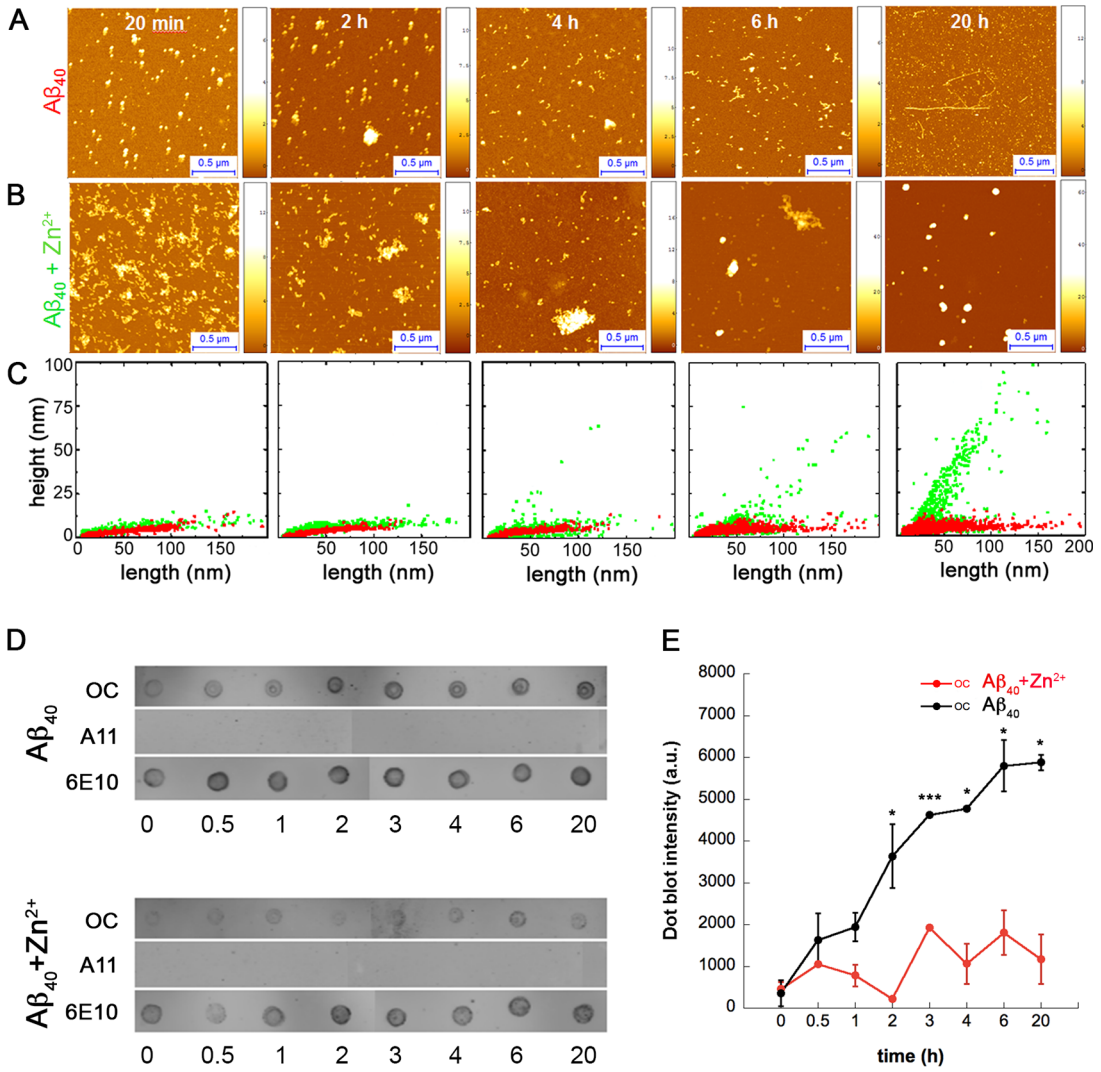

Figure 2. Aggregation of Aβ_{40} in the absence and presence of Zn^{2+}. AFM 3D morphology maps acquired at different time points (20 min, 2, 4, 6, and 20 h) from an ongoing aggregation reaction of Aβ_{40} in the absence (A) and presence (B) of Zn^{2+}. All the *z* scales (heights) are in nm. (C) Statistical analysis showing height versus length (in the case of spherical aggregates, length corresponds to diameter) of Aβ_{40} aggregates in the absence (red) and presence of Zn^{2+} (green). (D) Comparative time course of an aggregation reaction of Aβ_{40} in the absence and presence of Zn^{2+} probed with the conformation-specific antibodies OC and A11 and the sequence-specific antibody 6E10 used here as a control of concentration. One representative experiment is shown. (E) Quantification of the intensities of the dots probed with the OC antibody. The values are the means ± SEM of two independent experiments, and * $p \leq 0.05$, *** $p \leq 0.001$ relative to the samples of Aβ_{40} in the presence of Zn^{2+} at each time point.

Aliquots of aggregation reactions in the presence or in the absence of Zn^{2+} were taken at different time points (0, 0.5, 1, 2, 4, 6, and 20 h) and subjected to dot-blot assays with OC and A11 antibodies and, for control, with the 6E10 antibody, that is sequence-specific and binds to the N-terminus of Aβ_{40}. The images (Figure 2D) and the quantification of the intensity of the spots (Figure 2E) show that the species that are recognized by the OC antibody increased significantly over time when Aβ_{40} aggregated in the absence of Zn^{2+}, indicating the progressive formation of the fibrils, as also shown by the AFM images in Figure 2A. By contrast, in the presence of Zn^{2+}, the OC-reactive population was found to be stable and not to change its intensity over time. In the presence of Zn^{2+}, the aggregates gave rise to a weaker signal compared to those generated by incubating without Zn^{2+}. This reflects the fact that the aggregated species do not evolve to mature fibrils, but they are trapped in an oligomeric conformation state. No reactivity for the A11 antibody was detected both when Aβ_{40} was incubated in the absence and presence of Zn^{2+}, indicating that the Zn^{2+}-stabilized oligomers are homogeneous in their conformation and not significantly different in structure from the ones that form in the absence of Zn^{2+}. 6E10 was used as a control to make sure that the same amount of peptide was spotted on the membranes in each case (Figures 2D and E).

The aggregation kinetics of Aβ_{40} in the presence or absence of Zn^{2+} were also monitored by turbidimetry at 500 nm and by 8-anilinonaphthalene-1-sulfonate (ANS) binding to measure the turbidity and the hydrophobicity of the aggregated species, respectively (Figure S3). Since the beginning of the reaction, both the turbidity (Figure S3A) and ANS binding (Figures S3B–D) of the species forming in the presence of Zn^{2+} were higher than those observed for the species forming in the absence of Zn^{2+}, indicating the rapid formation of a population of aggregated species. Moreover, in the presence of Zn^{2+}, the turbidity and ANS binding signals were found not to

DOI: 10.1021/acschemneuro.8b00141
ACS Chem. Neurosci. 2018, 9, 2959–2971

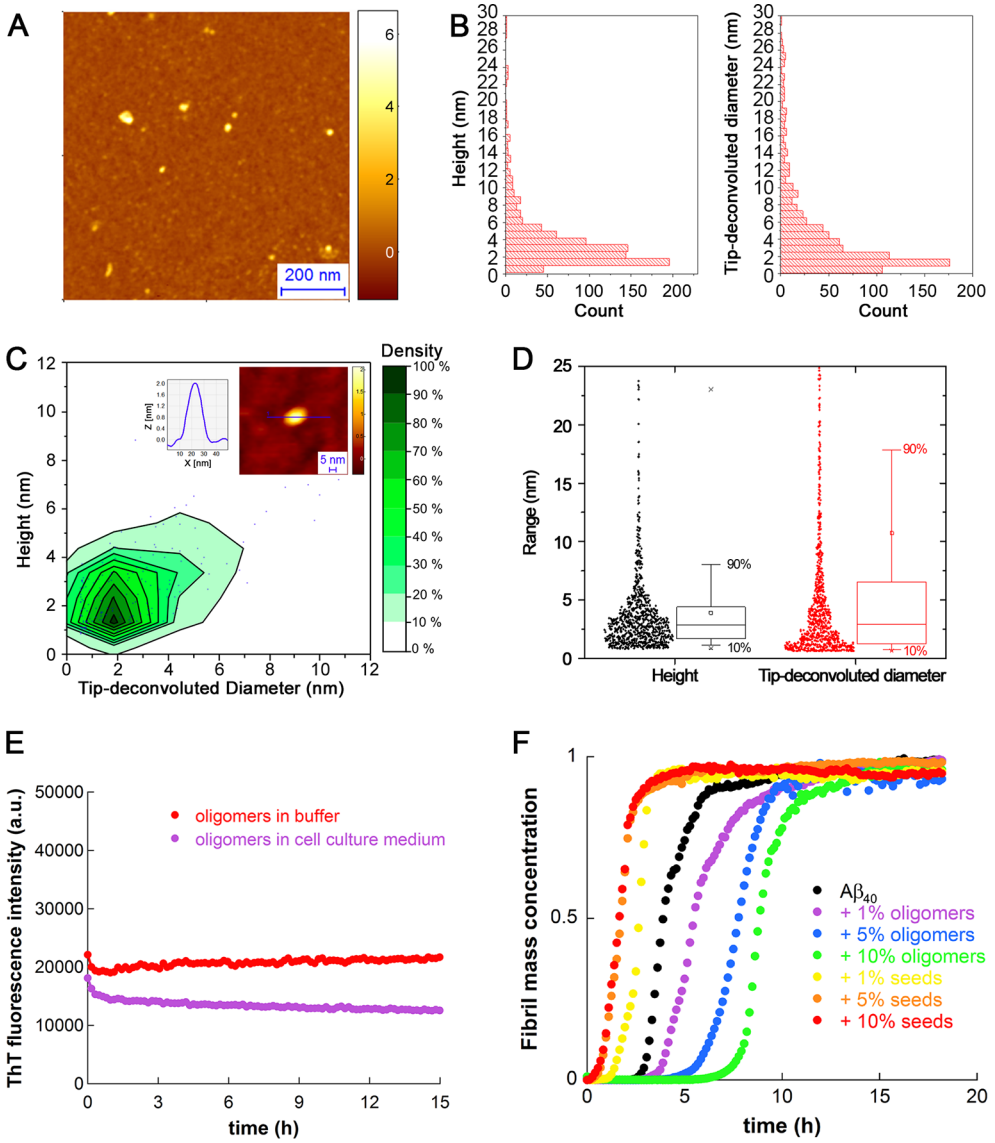

Figure 3. Structural homogeneity and stability of the Aβ_{40} oligomers generated in the presence of Zn^{2+}. (A) AFM morphology map of the oligomers isolated form the aggregation reaction in the presence of Zn^{2+}. (B) Cross-sectional size distributions of height (left) and tip-deconvoluted diameter (right). (C) Probability density map of the height versus the tip-deconvoluted diameter of the oligomers. Each point is a measurement of height and tip-deconvoluted diameter of individual oligomers. In the inset, the cross-section (x and z coordinates) and the image (x and y coordinates) of a representative oligomer of 2 nm height (z coordinate) is shown. (D) Box chart plots of height and tip-deconvoluted diameter with percentiles indicated. (E) ThT-based aggregation kinetics of preformed Aβ_{40} oligomers diluted either into buffer (red) or into cell culture medium (purple). (F) ThT-based aggregation kinetics of Aβ_{40} in the presence of preformed fibril seeds or preformed oligomers (1, 5, and 10%).

vary significantly over the 20 h of measurement (Figure S3), suggesting that the physicochemical properties of the aggregates remained stable over time, in agreement with the results obtained with the dot blot assay (Figures 2D and E).

Aβ_{40} Oligomers Stabilized by Zn^{2+} are Homogeneous and Stable. The aggregates obtained after 20 h of incubation in the presence of Zn^{2+} were centrifuged and resuspended in buffer. To evaluate the shape and size distribution of the resulting population, we acquire AFM images and performed a detailed statistical analysis. We measured the cross-sectional dimensions of the oligomeric species by taking into account their height and deconvoluted diameter[32] (see Experimental Procedures). The oligomers generated under the conditions described here were found to have a bead-like shape (Figure 3A) and a narrow size distribution with almost 80% of the population possessing an average cross-sectional diameter between 1 and 5 nm (Figures 3B–D). The narrow distribution of sizes obtained from the AFM data was also found to be consistent with measurements obtained in solution by means of dynamic light scattering (DLS) (Figure S4). The homogeneity of the Aβ_{40} oligomeric population obtained with our protocol is at variance with previous morphological studies of Aβ_{40} and Aβ_{42} aggregates in the presence of Zn^{2+} under different conditions, which have reported species characterized by nonfibrillar morphology, irregular shape, and broad distribution of sizes.[33−36] The centrifugation and resuspension steps of the protocol used in the present study are, however, very important as they allow a population of oligomers to be obtained with a size distribution that is much narrower than that observed for the population of aggregates obtained after 20 h of incubation and shown in the AFM images of Figure 2B and in the statistics of Figure 2C (green dots).

DOI: 10.1021/acschemneuro.8b00141
ACS Chem. Neurosci. 2018, 9, 2959−2971

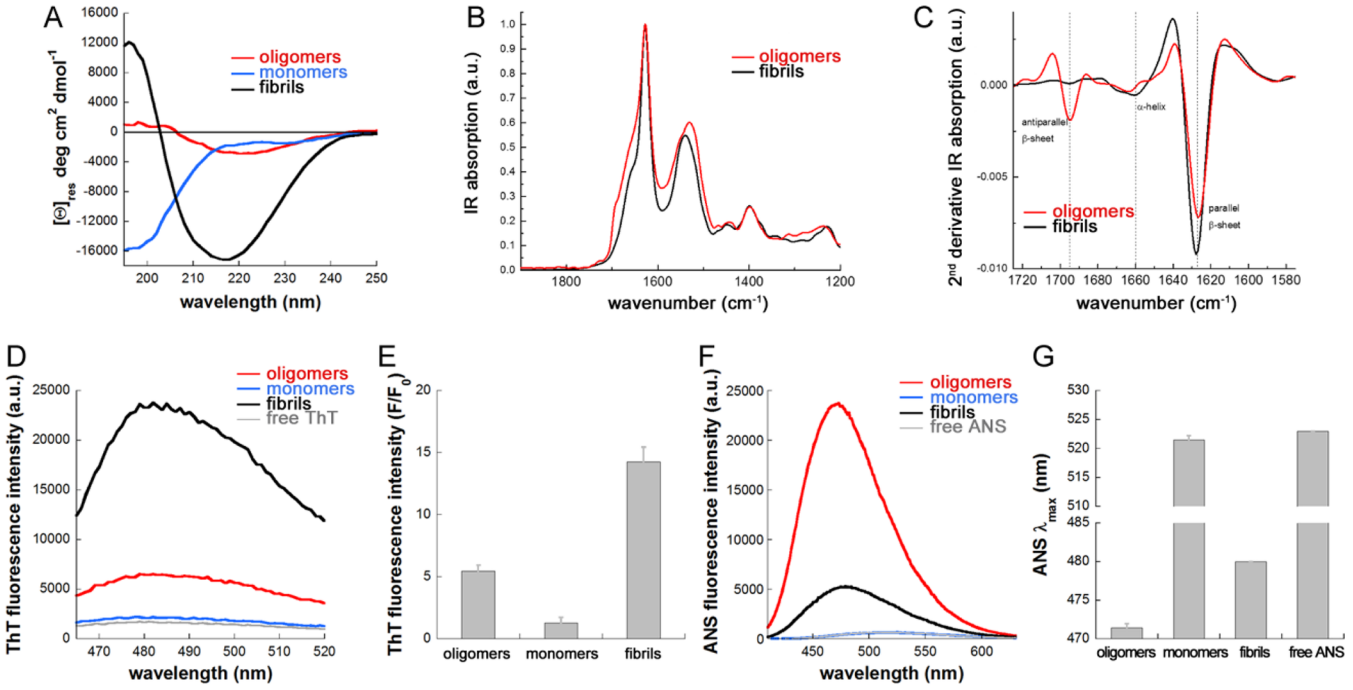

Figure 4. Structural characteristics of Aβ_{40} oligomers compared to monomers and fibrils. Far-UV CD (A), ATR-FTIR (B) and second derivative ATR-FTIR (C), ThT fluorescence (D) and ANS fluorescence spectra (F) of oligomeric (red line), monomeric (blue line), and fibrillar Aβ_{40} samples (black line) at the same concentration. The spectra of free ThT and ANS (gray line) in buffer are shown in panels D and F, respectively. (E) The F/F_0 ratio between the ThT fluorescence intensity at 485 nm in the presence (F) and absence (F_0) of protein obtained from the spectra in panel D. (G) The wavelength of maximum ANS emission fluorescence (λ_{max}) of the spectra in panel F. The error bars in panels E and G correspond to standard deviations from three different sets of experiments.

The stability of these oligomers was assessed with ThT-based kinetic experiments by incubating 10 μM oligomers (monomer equivalents) at 37 °C in 20 mM sodium phosphate buffer, pH 6.9, with 200 μM $ZnCl_2$ or cell culture medium. The results showed no changes in the ThT binding properties for as long as 15 h, suggesting that the oligomers are stable under these conditions. Indeed, no differences in the physicochemical properties of the oligomers could be observed when the oligomers were incubated in buffer or cell culture media (Figure 3E). This observation is particularly important in the context of experiments with cell cultures, as incubations are at 37 °C and last typically 24 h.

To test further the stability of these oligomers, we evaluated their ability to act as seeds for the aggregation process of Aβ_{40} at 37 °C (Figure 3F). The formation of Aβ_{40} fibrils was monitored in the presence of preformed fibrils and oligomers prepared with the protocol described in this study. The preformed fibrils accelerated the aggregation process of Aβ_{40} in accord with previous studies.[3,5] By contrast, the Aβ_{40} oligomers delayed further the aggregation of Aβ_{40} in a concentration-dependent manner (Figure 3F). Despite this delay in the kinetics of Aβ_{40} in the presence of the oligomers, no net decrease in the ThT values at the end of the aggregation reactions was observed (Figure S5A), indicating that the monomers eventually fully converted into fibrils and the final load of fibrils was unaltered by the oligomers. The comparison between the half-times of the aggregation kinetics measured with increasing concentrations of Zn^{2+} (Figure S1B) and the kinetics in the presence of the oligomers (Figure 3F) show that the inhibition effect is due to the presence of oligomers and not to the presence of the Zn^{2+} ions (Figure S5B). These data suggest that the inhibition of Aβ_{40} aggregation is primarily due to an intrinsic property of the oligomers to delay the aggregation, probably by kinetically trapping Aβ_{40} monomers and, at the same time, being unable to convert into mature fibrils. This latter effect is likely to increase the lifetime and potential toxic effects of the oligomers.

Structural Characteristics of the Zn^{2+}-Stabilized Aβ_{40} Oligomers. Using a range of different biophysical approaches, we characterized the secondary structure and tinctorial properties of the Zn^{2+}-stabilized Aβ_{40} oligomers and compared them with those of the monomeric and fibrillar species of Aβ_{40}. The far-UV circular dichroism (CD) spectrum of Aβ_{40} fibrils is typical of a polypeptide chain with high β-sheet structure content, which is characterized by positive ellipticity at 196 nm and negative ellipticity at 217 nm (Figure 4A). By contrast, the spectrum of the monomeric peptide is typical of that of disordered polypeptide chain, with a broad negative peak near 200 nm. The spectrum of the Zn^{2+}-stabilized Aβ_{40} oligomers, however, has a positive shoulder between 195 and 205 nm and a negative peak centered at 220 nm (Figure 4A), suggesting that these oligomers possess structural properties intermediate between those of the monomeric and the fibrillar species. A red-shift is also observed in the oligomer spectrum and can be attributed to the flattening effect of differential absorption, that can occur in suspensions containing aggregates.[37] The measurements were acquired at 25 μM concentration (monomer equivalents) for all the species.

The secondary structure of the Zn^{2+}-stabilized Aβ_{40} oligomers was also investigated by attenuated total reflection Fourier transform infrared (ATR-FTIR) spectroscopy. The position and the shape of the amide band I in the ATR-FTIR spectra of proteins are closely related to the secondary and quaternary structural organization of their polypeptide main

DOI: 10.1021/acschemneuro.8b00141
ACS Chem. Neurosci. 2018, 9, 2959−2971

chain. The amide band I region of the ATR-FTIR spectra of the different states of Aβ_{40} along with the second derivative spectra are shown in Figures 4B and C. The oligomers and the fibrils (2.8 mM monomer equivalents) both contain strong bands at 1625 and 1628 cm^{-1}, respectively, which can be assigned to the presence of intermolecular parallel β-sheet structure. In the case of the oligomeric aggregates, another strong component of the amide band I is visible at 1695 cm^{-1} and is related to the presence of antiparallel β-sheet structure. Deconvolution of the FTIR spectra shown in Figure S6 shows that this component represents ca. 15% of the total secondary structure in the oligomers, while it is almost absent in the fibrils. Such antiparallel β-sheet conformation has been reported to be a distinctive characteristic of oligomeric species of both Aβ_{40}[38−40] and Aβ_{42},[41,42] in contrast to the parallel β-sheet structure of mature fibrils.[42,43] This difference in the β-sheet geometry has been proposed to be a key factor in determining the rate of conversion of the oligomers into fibrils.[44] Indeed, the antiparallel structure could represent an energy barrier to the elongation, as the oligomers would need to rearrange their β-strands to a parallel conformation to growth into fibrils.[44] Finally, both mature fibrils and oligomers possess a weak band between 1630-1660 cm^{-1}, indicating a small fraction of α-helical and random coil conformation.

The presence of extensive β-sheet structure in Aβ_{40} oligomers and fibrils is consistent with their ability to bind ThT and increase its fluorescence (Figure 4D). However, the oligomers cause a 5-fold increment of ThT fluorescence with respect to the buffer solution, whereas in case of the fibrils the increase is almost 15-fold, as shown in Figure 4E. The Aβ_{40} monomers do not display any ThT binding as they do not cause any increase in the fluorescence of the dye. All the species were measured at 6 μM concentration (monomer equivalents). Taken together, these data suggest that the content of β-sheet structure of the oligomeric species is intermediate between that of the Aβ_{40} monomers and the fibrils.

We then sought to assess the degree of hydrophobic surface exposure using the fluorescent probe ANS. This dye binds to solvent-exposed hydrophobic surfaces, and this binding generates a strong increase in its fluorescence emission intensity and a blue shift of its maximum emission wavelength (λ_{max}).[45] Unlike Aβ_{40} monomers which have no effects on the ANS fluorescence, the oligomers and the fibrils (all the species at 40 μM concentration equivalent to the monomer) were both found to exhibit an increase in the fluorescence emission intensity of ANS (Figure 4F) and a blue shift of the maximum wavelength (λ_{max}) (Figure 4G). However, both these effects are much more marked in the oligomers with respect to the fibrils, indicating their higher degree of hydrophobic surface exposure; this structural parameter has been found to be particularly significant for cellular toxicity[46] as such exposure is thought to be an important factor affecting the physics of cellular membranes[47] and cellular proteins.[48]

Zn^{2+}-Stabilized Aβ_{40} Oligomers Cause Dysfunction in Neuroblastoma Cells. We evaluated the toxicity of the Zn^{2+}-stabilized Aβ_{40} oligomers formed using the protocol described here by means of four independent cellular assays, namely 3-(4,5-dimethylthiazol-2-yl)-2,5-diphenyltetrazolium bromide (MTT) reduction, trypan blue exclusion, resazurin reduction, and reactive oxygen species (ROS) production, with human neuroblastoma SH-SY5Y cell cultures (see Experimental Procedures). The oligomers were diluted into the cell culture medium and aliquots of the solution were then added to the cell cultures before performing the cell culture assays. As previously stated, Zn^{2+}-stabilized Aβ_{40} oligomers were found to be stable in the cell medium for at least 15 h using a ThT assay (Figure 3E).

The MTT test is a generic indicator of cellular dysfunction and stress,[49] monitoring the ability of metabolically active cells to reduce the MTT molecule through their mitochondria, a process that can be followed spectrophotometrically. The Aβ_{40} oligomers were found to decrease significantly the capacity of the SH-SY5Y cells to reduce the MTT molecule in a dose-dependent manner (Figure 5A). The decrease in the MTT reduction with respect to the untreated cells was 25 ± 3% at a concentration of 1 μM and increased to 35 ± 3 and 38 ± 5% at concentrations of 10 and 20 μM, respectively. This effect is comparable to that of oligomers formed by Aβ_{42}, islet amyloid polypeptide precursor (IAPP), HypF-N, and α-synuclein, which have been previously reported to display similar levels of toxicity with the same cell type.[47,50,51]

Analogous findings were obtained with the resazurin reduction inhibition assay, which takes advantage of the fact that healthy cells maintain a reducing environment within the cytosol and convert the nonfluorescent resazurin to the red and highly fluorescent resorufin. The results (Figure 5B) show that the aggregates were able to decrease the resazurin reduction by 12 ± 1 and 13 ± 2% at oligomer concentrations of 1 and 10 μM, respectively. Moreover, we carried out the trypan blue exclusion assay, which is based on the ability of viable cells to exclude the dye, but nonviable cells to be stained. The Aβ_{40} aggregates were found to cause cell death in a dose-dependent manner, with the level of toxicity being 15 ± 3 and 23 ± 4% at concentrations of 1 and 10 μM, respectively (Figure 5C).

Finally, we measured ROS production after exposing neuroblastoma cells to the oligomers (Figures 5D and E). The generation of intracellular ROS leads to perturbations of proteins, membrane lipids, and nucleic acids in the cells, and it is therefore a cause of cellular dysfunction. This phenomenon has been associated with the damage caused by oligomers generated from different peptides and proteins, including Aβ and α-synuclein.[14,44] Aβ_{40} oligomers, when added to neuroblastoma cells, induced a dose-dependent increase of ROS production levels over time at room temperature, whereas the corresponding concentrations of buffer containing $ZnCl_2$ did not trigger the release of ROS (Figure 5D). At a concentration of 20 μM, the oligomers reached a 6-fold increase of ROS production relative to the buffer after 2 h of incubation at room temperature (Figure 5E). Taken together, these data all show the toxic nature of the Zn^{2+}-stabilized Aβ_{40} oligomers.

Zn^{2+}-Stabilized Aβ_{40} Oligomers Cause Dysfunction in *C. elegans*. We further evaluated the biological effect of Aβ_{40} oligomers by using the animal model *C. elegans*. Due to its simple anatomy and short lifespan, in combination with well-established genetics, the 1 mm long nematode worm *C. elegans* has become an extremely powerful model organism in biomedical research, spanning applications from reverse genetics to drug discovery.[51−53] Wild-type N2 worms[54] were exposed to increasing concentrations of oligomers and screened for phenotypic readouts such as body bends per minute (BPM) and the speed of movement.[55] These parameters are well-established indicators of the fitness of the worms. We found that, after the treatment with the oligomers, the frequency of the body bends (Figure 6A) and their speed (Figure 6B) were markedly reduced compared to the untreated worms at all the concentrations tested, reaching at 30 μM oligomer

DOI: 10.1021/acschemneuro.8b00141
ACS Chem. Neurosci. 2018, 9, 2959−2971

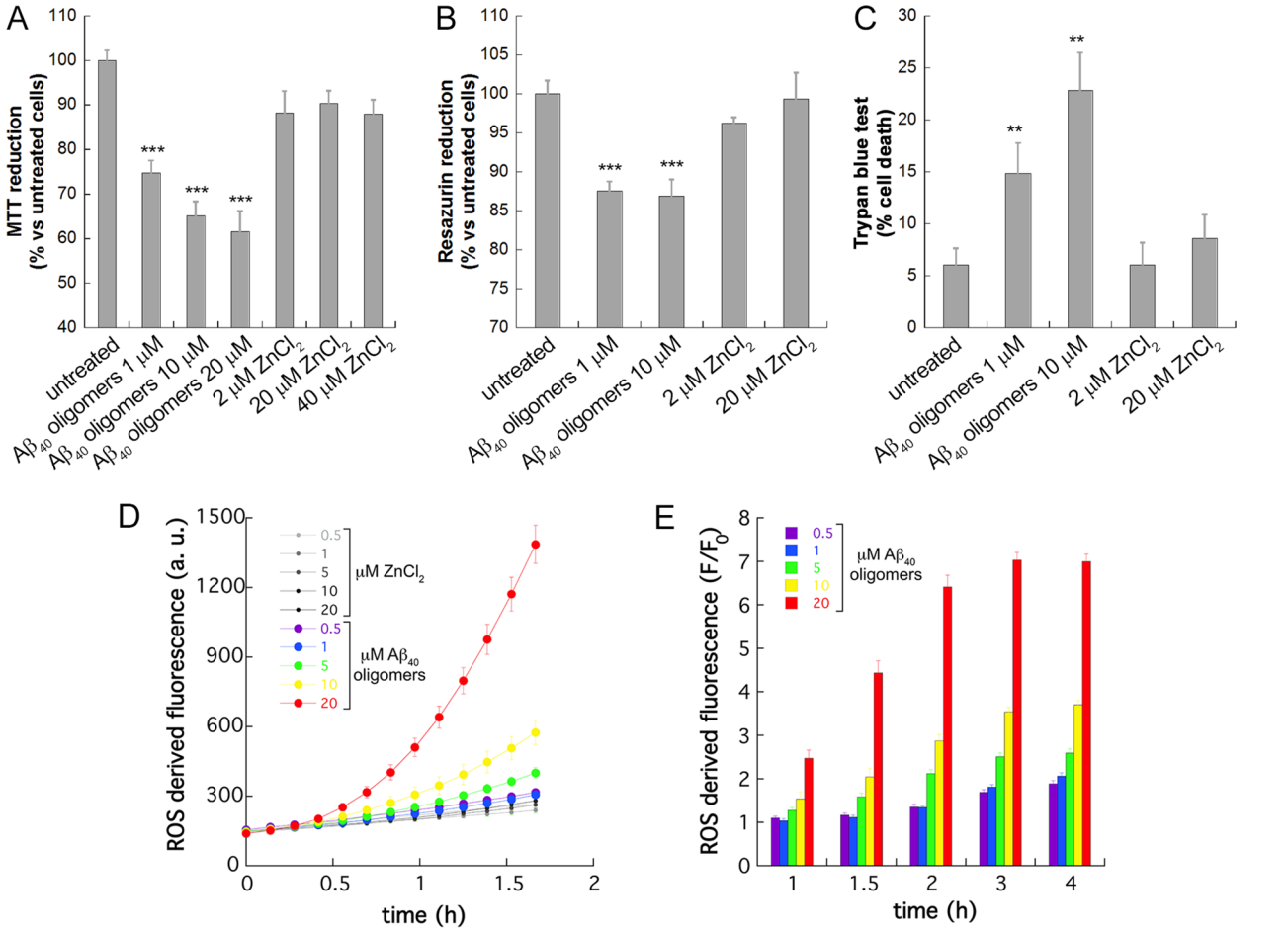

Figure 5. Cytotoxicity of Aβ_{40} oligomers prepared in the presence of Zn2+ in human neuroblastoma SH-SY5Y cell cultures. (A) Cell viability determined by the MTT reduction test in cells exposed to different concentrations of the Aβ_{40} oligomers and the corresponding controls (buffer containing Zn2+). The values reported are means ± SEM and were determined from four independent experiments. (B) Resazurin reduction assay in cells treated with different concentrations of the Aβ_{40} oligomers and the corresponding controls. The values reported are means ± SEM and were determined from 12 replicas in the same experiment. (C) Percentage of cell deaths estimated by the trypan blue test in cells exposed to different concentrations of the Aβ_{40} oligomers and the corresponding controls. The results reported are means ± SEM and were determined from 12 replicas in the same experiment. The data are expressed as the percentage of cell death obtained with 70% ethanol for 15 min. (D) Kinetics of ROS production at room temperature following the treatment of the cells with different concentrations of the Aβ_{40} oligomers and the corresponding controls. (E) F/F_0 ratio between the ROS derived fluorescence intensity in the presence (F) and absence (F_0) of different concentration of the Aβ_{40} oligomers taken at different time points. Error bars in panels D and E are SEM and were obtained from 6 replicas in the same experiment. In the panels, * $p \leq 0.05$, ** $p \leq 0.01$, *** $p \leq 0.001$ relative to untreated cells are shown.

concentration a decrease of 21 ± 4% in the BPM and a reduction of 17 ± 3% in the speed of movements (Figures 6 A and B).

As a further proof of the toxicity of the Aβ_{40} oligomers in *C. elegans*, we assessed the production of ROS in the worms following the treatment with different concentrations of oligomers, taking advantage of a luminescence-based assay that measures the levels of hydrogen peroxide directly in the tissues (Figure 6C). Aβ_{40} oligomers were found to induce a dose-dependent increase of ROS production levels. At a concentration of 30 μM, the oligomers were able to stimulate a 3-fold increase of ROS production compared to the untreated worms (Figure 6C).

Confocal microscopy images (Figure 6D) of worms treated with fluorescein-5-isothiocyanate (5-FITC) labeled oligomers were acquired to gain insight into the interactions between the oligomers and the worms. The images revealed that the oligomers can penetrate the membranes of the cells forming the intestinal walls and diffuse in the internal tissues, therefore exerting toxic effects on the worms (Figure 6D).

CONCLUSIONS

We here described a protocol to generate stable Aβ_{40} oligomers based on the introduction of Zn^{2+} in an aggregation reaction carried out under near-native conditions. This method is non-invasive, as it does not involve covalent modifications of the Aβ_{40} peptide and, considering that Zn^{2+} is an abundant metabolite in the brain, results in oligomers that may resemble at least some of those that occur *in vivo*.

The mechanism of formation of these oligomers was monitored by several techniques, including single molecule AFM at different time points of the aggregation process. Under the condition that we used, the presence of Zn^{2+} inhibits the formation of mature fibrils and provides a population of smaller aggregates. These aggregates are conformationally similar to the naturally occurring oligomers that form in the aggregation process of Aβ_{40} in the absence of Zn^{2+}, as they show the same reactivity to the OC conformation-specific antibody. The centrifugation and resuspension of the aggregates formed in the presence of Zn^{2+} allow the isolation of a population of

DOI: 10.1021/acschemneuro.8b00141
ACS Chem. Neurosci. 2018, 9, 2959−2971

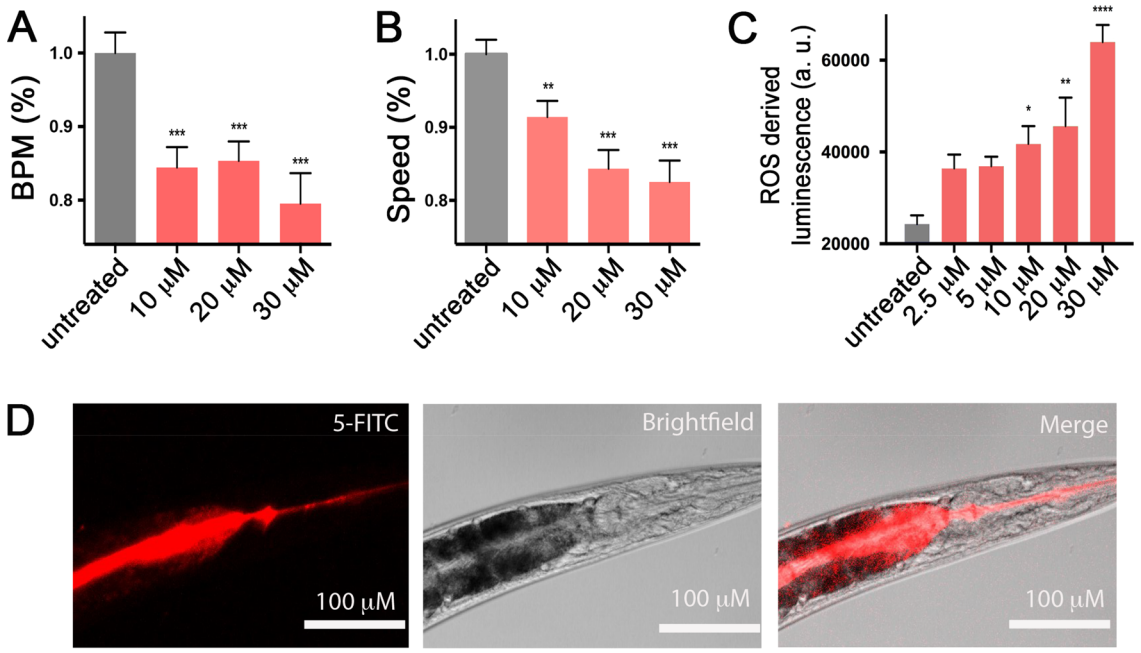

Figure 6. Cytotoxicity of the stabilized Aβ_{40} oligomers in *C. elegans*. Different concentrations of the oligomers were administered to the animals at a day 0 of adulthood, and 300 animals were analyzed per condition in 3 different replicas. The BPM (A) and speed of the movement (B) of the treated worms were compared to those of untreated worms. (C) ROS production was measured after the exposure of the worms to different concentration of oligomers using a luminescence-based assay that measures the level of hydrogen peroxide directly in tissues. One experiment representative of 3 is shown. Student-*t* tests were carried out, and in the panels, * $p \leq 0.05$, ** $p \leq 0.01$, *** $p \leq 0.001$, **** $p \leq 0.0001$ relative to untreated worms are reported. (D) Representative confocal microscopy (left), bright-field (center), and merged (right) images of worms treated for 12 h with 30 μM stabilized Aβ_{40} oligomers labeled with 5-FITC.

oligomers that is largely homogeneous and has a narrow size distribution, with the 80% of the species in the 1−5 nm range of dimensions. The oligomers were found to be stable and incapable of growing into fibrils at a detectable rate, as previously observed for other OC-positive Aβ_{40} oligomers.[56] The biophysical characterization of these oligomers has revealed that they have a β-sheet content intermediate between that of the monomeric and the fibrillar species, as assessed by CD, ThT binding, and FTIR. This latter technique shows that the oligomers posses some antiparallel β-sheet structure, which has been observed to be a distinctive sign for early oligomeric species of Aβ.[38,41,57] This antiparallel geometry could explain why these oligomers are stable, kinetically trapped in this intermediate state, and hence unable to elongate into fibrils where the parallel β-sheets are observed. Indeed, the β-sheet geometry has been found to play an important role in the stability of other oligomeric systems, e.g. the oligomers of α-synuclein, which were also found to have antiparallel β-sheet structure and to be much less prone to grow by addition of monomers with respect to the fibrils that are readily able to increase in length.[44] The Aβ_{40} oligomers stabilized by Zn^{2+} have high surface hydrophobicity which, together with their small size, is a key property for determining their toxicity.[46,50,58] Indeed, we have found that these oligomers decrease the viability of neuroblastoma cells and are able to significantly impair the motility of *C. elegans* models.

We have thus shown that these Zn^{2+}-stabilized Aβ_{40} oligomers generated with this protocol have high stability, structural homogeneity, and are toxic. We anticipate that the availability of Aβ_{40} oligomers formed under conditions mimicking the oligomerization environment *in vivo* and having the expected biophysical properties of cytotoxic oligomers provides a unique tool for the investigation of the molecular origins of cellular toxicity in Alzheimer's disease.

EXPERIMENTAL PROCEDURES

Production of Aβ_{40} Peptides. Expression and purification of the recombinant Aβ (M1-40) peptide (MDAEFRHDSGYEVHHQKLVFFAEDVGSNKGAIIGLMVGGVV), denoted Aβ_{40}, was carried out as previously described for Aβ_{42}.[53] Briefly, Aβ_{40} was expressed in the *Escherichia coli* BL21Gold (DE3) strain (Stratagene, La Jolla, CA) and purified by sonicating the bacterial cells and dissolving the inclusion bodies in 8 M urea, followed by ion exchange in batch mode on diethylaminoethyl cellulose resin. The fractions were lyophilized and further purified using a Superdex 75HR 26/60 column (GE Healthcare, Chicago, IL), and eluates were analyzed using SDS−polyacrylamide gel electrophoresis for the presence of the desired protein product. The fractions containing the recombinant protein were combined, frozen using liquid nitrogen, lyophilized in 50 mM ammonium acetate, pH 8.5, and stored at −80 °C.

Preparation of Zn^{2+}-Stabilized Aβ_{40} Oligomers. To generate stable Aβ_{40} oligomers, 1 mg of the lyophilized Aβ_{40} peptide was dissolved in 300 μL of 100% HFIP overnight at 4 °C, and the solvent was then allowed to evaporate under a gentle flow of N_2. The peptide was resuspended in DMSO at a concentration of 2.2 mM and sonicated twice for 10 min at room temperature. The Aβ_{40} peptide was then diluted in 20 mM sodium phosphate buffer, at pH 6.9, with 200 μM $ZnCl_2$ to a final concentration of Aβ_{40} of 100 μM, incubated at 20 °C for 20 h in a final volume of 275 μL and centrifuged at 15 000*g* for 15 min at 20 °C. The pellet containing the oligomers was resuspended in 20 mM phosphate buffer at pH 6.9, with 200 μM $ZnCl_2$. The concentration of the oligomers was determined by measuring the absorbance at 280 nm using the theoretical molar extinction coefficient ε_{280} = 1490 M^{-1} cm^{-1},[59] and is expressed throughout the text as equivalent to the concentration of the monomers.

Preparation of Aβ_{40} Monomers and Fibrils. Solutions of the monomeric peptide were prepared by dissolving the lyophilized Aβ_{40} peptide in 6 M guanidinium hydrocholoride. The monomers were purified from any oligomeric species and salts using a Superdex 75 10/300 GL column (GE Healthcare, Chicago, IL) at a flow rate of 0.5 mL/min and eluted in 20 mM sodium phosphate buffer at pH 8.

DOI: 10.1021/acschemneuro.8b00141
ACS Chem. Neurosci. 2018, 9, 2959−2971

The center of the peak was collected, and the peptide concentration determined from the absorbance of the integrated peak area using ε_{280} = 1490 M^{-1} cm^{-1}. For the preparation of Aβ_{40} fibrils, Aβ_{40} was incubated for 10 h at the concentration of 50 μM in 20 mM sodium phosphate buffer, pH 8, at 37 °C in a 96-well plate. Part of these samples was supplemented with a solution of 20 μM ThT to monitor the aggregation of the samples with ThT kinetic. Samples not treated with ThT were then collected from the wells into low-binding tubes.

Atomic Force Microscopy. AFM was performed on freshly cleaved, positively functionalized mica substrates. The functionalization was performed by incubating the substrates for 1 min with 10 μL of a solution 0.5% (v/v) (3-aminopropyl)triethoxysilane (APTES) in water, rinsing with 1 mL of water for 3 times, and drying under a gentle flow of nitrogen. Before the deposition on the substrate, the oligomeric preparations were diluted 10 times in water. In another set of experiments, Aβ_{40} was incubated at 100 μM in 20 mM phosphate buffer at pH 6.9 in the presence or absence of 200 μM Zn^{2+}, and aliquots of the aggregation mixtures were taken at different time points and diluted 10 times in water. Ten microliter aliquots of each diluted sample were deposited on the functionalized mica at room temperature, incubated for 10 min, rinsed with 1 mL water, and then dried under a gentle nitrogen flow. AFM maps were generated by means of a JPK nanowizard2 system (JPK Instruments, Berlin, Germany) operating in tapping mode and equipped with a silicon tip (mmasch, 2 N m^{-1}) with a nominal radius of 10 nm. Image flattening and single aggregate statistical analysis was performed by SPIP software (Image Metrology, Hørsholm, Denmark). While the geometry of the AFM tip does not strongly affect the height measurement of the observed object, it is the primary determinant of the lateral resolution. Indeed, a tip with an apical radius of the same size, or larger than the dimensions of the object under investigation, will affect the measurement of the diameter because of the so-called convolution effect,[32] resulting in an enlargement of the lateral dimensions. In the present experiments, objects with typical lateral dimensions within 1−10 nm were measured by a tip radius of approximately 10 nm. For this reason, we quantified the deconvoluted diameter of the aggregates as described previously.[32]

Dot-Blot Assay. Aβ_{40} monomers in DMSO were diluted at 100 μM in 20 mM phosphate buffer at pH 6.9 in the presence or absence of 200 μM Zn^{2+}. From these aggregation mixtures, aliquots were taken at different time points, diluted 20 times in 20 mM phosphate buffer at pH 6.9, and spotted (2 μL) on a nitrocellulose membrane with a pore size of 0.2 μm. The membranes were blocked for 1 h (PBS, 0.1% tween, 5% milk), incubated overnight with 1:1000 6E10 (Biolegend, San Diego, CA), 1:1000 OC (Merck, Darmstadt, Germany), and 1:750 A11 (Invitrogen, Carlsbad, CA) primary antibodies diluted in blocking solution, and then incubated for 1 h with Alexa488-conjugated secondary antibodies diluted in blocking solution at 1:5000. After each incubation, the membranes were washed in PBS, 0.1% tween. Fluorescence was detected using a Typhoon Trio Imager (GE Healthcare, Chicago, IL). Quantification was performed using ImageJ software (NIH, Bethesda, MD).

ThT Binding Assays. To check their stability, preformed oligomers were diluted to a final concentration of 10 μM into either 20 mM sodium phosphate buffer, pH 6.9, with 200 μM $ZnCl_2$ or cell culture medium, both equilibrated at 37 °C in the presence of 40 μM ThT, and placed in a 96-well plate at 37 °C for 15 h. The ThT fluorescence signals (excitation at 440 nm, emission at 480 nm) were recorded using a plate reader (BMG Labtech, Aylesbury, UK). In the seeded experiments, a freshly purified solution of Aβ_{40} monomers was diluted at 30 μM concentration in 20 mM sodium phosphate buffer at pH 8 in the presence of 20 μM ThT. All samples were prepared in low binding Eppendorf tubes on ice. Each sample was then pipetted into multiple wells of a 96-well half area, low-binding, clear bottomed and PEG coated plate (Corning 3881, Corning, NY), 80 μL per well, in the absence and the presence of 1%, 5%, or 10% concentrations of either fibril seeds or oligomers from Aβ_{40}. Preformed fibrils and oligomers were prepared as described above and added just before the experiment to the freshly prepared monomer solution. Kinetic assays were obtained by placing the 96-well plate at 37 °C under quiescent conditions in a plate reader using the settings described above. In the experiment to allow the comparison of oligomeric, monomeric, and fibrillar Aβ_{40} species, 6 μM (monomer equivalents) aliquots of each sample were added to solutions of 25 μM ThT dissolved in 20 mM phosphate buffer at pH 6.9. The emission spectra were recorded at 37 °C using a plate reader (excitation at 440 nm).

Circular Dichroism. Far-UV CD spectra of oligomeric, monomeric, and fibrillar Aβ_{40} were acquired using a 1 mm path length quartz cuvette and a J-810 spectropolarimeter (Jasco, Tokyo, Japan) equipped with a Peltier thermally controlled cuvette holder at 20 °C. The concentration of each sample was 25 μM (monomer equivalents). Spectra were obtained by averaging 5 scans recorded in the 185−250 nm wavelength range using a scanning speed of 50 nm/min and a data pitch of 1 nm. The averaged spectra were smoothed using the "means-movement" procedure implemented in the Spectra Manager package. For each sample, the CD signal of the buffer was subtracted from the CD signal of the protein.

Fourier Transform Infrared Spectroscopy. Oligomeric and fibrillar Aβ_{40} samples were centrifuged and the pellets resuspended in 10 μL of H_2O to achieve a final protein concentration of 2.8 mM (monomer equivalents). ATR-FTIR spectroscopy was performed using a Bruker Vertex 70 spectrometer equipped with a diamond ATR element (Bruker, Billerica, MA). Spectra were acquired with a resolution of 4 cm^{-1} and processed by means of Origin Pro software. For each sample, 3 spectra were averaged (each spectrum obtained from 128 scans), and then the second derivative was calculated applying a Savitzky−Golay filter (2nd order, 12 points).

ANS Binding Assay. Forty micromolar (monomer equivalents) aliquots of oligomeric, monomeric or fibrillar Aβ_{40} were added to solutions of ANS in 20 mM phosphate buffer at pH 6.9 to obtain a 3-fold excess of dye. The emission spectra (excitation at 380 nm) were recorded at 37 °C using a plate reader (BMG Labtech, Aylesbury, UK).

Cell Cultures. Human SH-SY5Y neuroblastoma cells (A.T.C.C., Manassas, VA) were cultured in Dulbecco's modified Eagle's medium (DMEM)-F12+GlutaMax supplement (Thermo Fisher Scientific, Waltham, MA) with 10% fetal bovine serum. The cell cultures were maintained in a 5.0% CO_2 humidified atmosphere at 37 °C and grown until 80% confluence for a maximum of 20 passages.

MTT, Resazurin, and Trypan Blue Assays. SH-SY5Y cells were transferred into a 96-well plate and treated for 24 h at 37 °C in the absence or presence of different concentrations of the Aβ_{40} oligomers. After this incubation, the cells were subjected to different protocols to evaluate their health status. In the MTT test,[49] the cell cultures were incubated with 0.5 mg/mL MTT solution at 37 °C for 4 h and subsequently with cell lysis buffer (20% SDS, 50% *N*,*N*-dimethylformamide, pH 4.7) at 37 °C for 3 h. Absorbance values of blue formazan were determined at 590 nm using a plate reader (BMG Labtech, Aylesbury, UK), and cell viability was expressed as the percentage of MTT reduction in treated cells as compared to untreated cells (taken as 100%). In the Resazurin assay, 10 μL of a 10× solution of alamarBlue (Invitrogen, Carlsbad, CA) was added according to the manufacturer's protocol into each well, and the plate was incubated for 4 h at 37 °C. The reduction of resazurin to resorufin was monitored by measuring the emission of fluorescence at 588 (excitation at 560 nm) at 37 °C using a plate reader (BMG Labtech, Aylesbury, UK), and cell viability was expressed as the percentage of resazurin reduction in treated cells relative to untreated cells. In the trypan blue assay,[60] a sterile 0.4% trypan blue solution was added to a final concentration of 0.05% to each well, and the plate was placed at 37 °C for 15 min. Dye containing media was removed by three washings with ice-cold PBS, and the cells were then lysed with 100 μL of lysis buffer (20% SDS, 50% *N*,*N*-dimethylformamide, pH 4.7) for 1 h at 37 °C. The absorbance values of the trypan blue were analyzed spectrophotometrically at 590 nm using a plate reader (BMG Labtech, Aylesbury, UK). The resulting data are expressed as percentages of the cell death obtained by treatment with 70% ethanol for 15 min. In all three assays, data were expressed as the mean ± standard error of the mean (SEM). Comparisons between group pairs were performed using the Student's *t* test. A *p*-value lower than 0.05 was

DOI: 10.1021/acschemneuro.8b00141
ACS Chem. Neurosci. 2018, 9, 2959−2971

considered statistically significant. p-values <0.05, <0.01 and <0.001 are indicated by single, double, and triple asterisks, respectively.

Measurement of ROS Production. The ROS production was measured using the Fluorometric Intracellular ROS kit MAK143 (Sigma-Aldrich, St. Louis, MO) according to the manufacturer's protocol. In brief, SH-SY5Y cells were seeded in black polystyrene 96-well plates for 24 h, and then were treated in the absence or in the presence of $A\beta_{40}$ oligomers at concentrations of 0.5, 1, 5, 10, and 20 μM. The ROS production was monitored over time by measuring the emission of fluorescence at 520 (excitation at 490 nm) at room temperature using a plate reader (BMG Labtech, Aylesbury, UK).

***C. elegans* Strain and Procedures.** *C. elegans* Bristol (N2) strain was used.[54] The animals were synchronized by hypochlorite bleaching, hatched overnight in M9 buffer (3 g/L KH_2PO_4, 6 g/L Na_2HPO_4, 5 g/L NaCl, 1 μM $MgSO_4$), and subsequently cultured at 20 °C on nematode growth medium (NGM) ($CaCl_2$ 1 mM, $MgSO_4$ 1 mM, 5 μg/mL cholesterol, 250 μM KH_2PO_4 pH 6, 17 agar g/L, 3g/l NaCl, 7.5 g/L casein) plates seeded with the *E. coli* strain OP50. On day 3 after synchronization, worms were placed on NGM plates containing 75 μM 5-fluoro-2′deoxy-uridine (FUDR) to inhibit the growth of offspring.

Automated Motility Assay. About 300 *C. elegans* worms at day 0 of adulthood were incubated in M9 buffer in the absence or in the presence of different concentrations of $A\beta_{40}$ oligomers for up to 12 h under gentle shaking. After the incubation, the worms were plated on agar plates and analyzed in an automated way[55] for fitness dysfunctions using a homemade microscopic setup. Motility procedures were carried out after 6 h incubation. All experiments were carried out in triplicate.

Measurement of ROS in *C. elegans*. About 200 worms were incubated in M9 buffer in the absence or in the presence of different concentrations of $A\beta_{40}$ oligomers for 5 h under gentle shaking. After the incubation, the worms were subjected to measurement of ROS production using the ROS-Glo H_2O_2 kit (Promega, Madison, WI) following the manufacturer's instructions. The luminescence was measured with a plate reader (BMG Labtech, Aylesbury, UK). All experiments were carried out in triplicate and one representative experiment of three is shown.

Confocal Microscope Imaging in *C. elegans*. $A\beta_{40}$ oligomers were buffer exchanged in PBS at pH 7.4, labeled with the probe 5-FITC using the AnaTag 5-FITC Microscale Protein Labeling Kit (AnaSpec, San Jose, CA), and then incubated at 30 μM with worms. Imaging was carried out after 12 h of incubation, using a Leica SP8 confocal microscope (Leica Microsystems, Wetzlar, Germany) at a nominal magnification of 20×; for each picture, 20 stacks of 0.7 μm/each were acquired. At least 30 animals were examined per condition. All experiments were carried out in triplicate, and the data from one representative experiment are shown in the figure.

■ ASSOCIATED CONTENT

Supporting Information

The Supporting Information is available free of charge on the ACS Publications website at DOI: 10.1021/acschemneuro.8b00141.

Additional figures and methods (PDF)

■ AUTHOR INFORMATION

Corresponding Author

*E-mail: mv245@cam.ac.uk.

ORCID

Michele Perni: 0000-0001-7593-8376

Tuomas P. J. Knowles: 0000-0002-7879-0140

Michele Vendruscolo: 0000-0002-3616-1610

Author Contributions

B.M., J.H., S.C., F.S.R., M.P., C.M.D., T.P.J.K., and M.V. designed research; B.M., J.H., S.C., F.S.R., and M.P. performed research. B.M., J.H., S.C., F.S.R., M.P., C.M.D., T.P.J.K., and M.V. analyzed data, and B.M., J.H., S.C., F.S.R., M.P., C.M.D., T.P.J.K., and M.V wrote the paper.

Notes

The authors declare no competing financial interest.

■ ACKNOWLEDGMENTS

This work was supported by the Cambridge Centre for Misfolding Diseases (B.M., J.H., S.C., F.S.R., M.P., T.P.J.K., C.M.D, and M.V.), the Swiss National Science Foundation for Science (Grant P300P2_171219 and P2ELP2_162116) and Darwin College (F.S.R.), the Frances and Augustus Newman Foundation (T.P.J.K.), the UK Biotechnology and Biochemical Sciences Research Council (M.V. and C.M.D.), the Wellcome Trust (T.P.J.K, C.M.D. and M.V.).

■ REFERENCES

(1) Chiti, F., and Dobson, C. M. (2017) Protein Misfolding, Amyloid Formation, and Human Disease: A Summary of Progress over the Last Decade. *Annu. Rev. Biochem. 86* (1), 27−68.

(2) Eisenberg, D., and Jucker, M. (2012) The Amyloid State of Proteins in Human Diseases. *Cell 148* (6), 1188−1203.

(3) Knowles, T. P. J., Vendruscolo, M., and Dobson, C. M. (2014) The Amyloid State and Its Association with Protein Misfolding Diseases. *Nat. Rev. Mol. Cell Biol. 15* (6), 384−396.

(4) Sunde, M., Serpell, L. C., Bartlam, M., Fraser, P. E., Pepys, M. B., and Blake, C. C. F. (1997) Common Core Structure of Amyloid Fibrils by Synchrotron X-Ray Diffraction. *J. Mol. Biol. 273* (3), 729−739.

(5) Knowles, T. P. J., Waudby, C. A., Devlin, G. L., Cohen, S. I. A., Aguzzi, A., Vendruscolo, M., Terentjev, E. M., Welland, M. E., and Dobson, C. M. (2009) An Analytical Solution to the Kinetics of Breakable Filament Assembly. *Science 326* (5959), 1533−1537.

(6) Bemporad, F., and Chiti, F. (2012) Protein Misfolded Oligomers: Experimental Approaches, Mechanism of Formation, and Structure-Toxicity Relationships. *Chem. Biol. 19* (3), 315−327.

(7) Haass, C., and Selkoe, D. J. (2007) Soluble Protein Oligomers in Neurodegeneration: Lessons from the Alzheimer's Amyloid β-Peptide. *Nat. Rev. Mol. Cell Biol. 8* (2), 101−112.

(8) Billings, L. M., Oddo, S., Green, K. N., McGaugh, J. L., and LaFerla, F. M. (2005) Intraneuronal Aβ Causes the Onset of Early Alzheimer's Disease-Related Cognitive Deficits in Transgenic Mice. *Neuron 45* (5), 675−688.

(9) Bucciantini, M., Giannoni, E., Chiti, F., Baroni, F., Formigli, L., Zurdo, J., Taddei, N., Ramponi, G., Dobson, C. M., and Stefani, M. (2002) Inherent Toxicity of Aggregates Implies a Common Mechanism for Protein Misfolding Diseases. *Nature 416* (6880), 507−511.

(10) Cleary, J. P., Walsh, D. M., Hofmeister, J. J., Shankar, G. M., Kuskowski, M. A., Selkoe, D. J., and Ashe, K. H. (2005) Natural Oligomers of the Amyloid-β Protein Specifically Disrupt Cognitive Function. *Nat. Neurosci. 8* (1), 79−84.

(11) Koffie, R. M., Meyer-Luehmann, M., Hashimoto, T., Adams, K. W., Mielke, M. L., Garcia-Alloza, M., Micheva, K. D., Smith, S. J., Kim, M. L., Lee, V. M., et al. (2009) Oligomeric Amyloid β Associates with Postsynaptic Densities and Correlates with Excitatory Synapse Loss near Senile Plaques. *Proc. Natl. Acad. Sci. U. S. A. 106* (10), 4012−4017.

(12) Lesné, S., Koh, M. T., Kotilinek, L., Kayed, R., Glabe, C. G., Yang, A., Gallagher, M., and Ashe, K. H. (2006) A Specific Amyloid-β Protein Assembly in the Brain Impairs Memory. *Nature 440* (7082), 352−357.

(13) Winner, B., Jappelli, R., Maji, S. K., Desplats, P. A., Boyer, L., Aigner, S., Hetzer, C., Loher, T., Vilar, M., Campioni, S., et al. (2011) In Vivo Demonstration That α-Synuclein Oligomers Are Toxic. *Proc. Natl. Acad. Sci. U. S. A. 108* (10), 4194−4199.

(14) Fändrich, M. (2012) Oligomeric Intermediates in Amyloid Formation: Structure Determination and Mechanisms of Toxicity. *J. Mol. Biol. 421* (4−5), 427−440.

DOI: 10.1021/acschemneuro.8b00141
ACS Chem. Neurosci. 2018, 9, 2959−2971

(15) Williams, A. D., Sega, M., Chen, M., Kheterpal, I., Geva, M., Berthelier, V., Kaleta, D. T., Cook, K. D., and Wetzel, R. (2005) Structural Properties of Aβ Protofibrils Stabilized by a Small Molecule. *Proc. Natl. Acad. Sci. U. S. A. 102* (20), 7115−7120.
(16) Bitan, G., and Teplow, D. B. (2004) Rapid Photochemical Cross-Linking - a New Tool for Studies of Metastable, Amyloidogenic Protein Assemblies. *Acc. Chem. Res. 37* (6), 357−364.
(17) Sandberg, A., Luheshi, L. M., Pereira de Barros, T., Macao, B., Knowles, T. P. J., Biverstål, H., Lendel, C., Ekholm-Petterson, F., Dubnovitsky, A., Lannfelt, L., et al. (2010) Stabilization of Neurotoxic Alzheimer Amyloid-β Oligomers by Protein Engineering. *Proc. Natl. Acad. Sci. U. S. A. 107* (35), 15595−15600.
(18) Näslund, J., Schierhorn, A., Hellman, U., Lannfelt, L., Roses, A. D., Tjernberg, L. O., Silberring, J., Gandy, S. E., Winblad, B., Greengard, P., et al. (1994) Relative Abundance of Alzheimer Aβ Amyloid Peptide Variants in Alzheimer Disease and Normal Aging. *Proc. Natl. Acad. Sci. U. S. A. 91* (18), 8378−8382.
(19) Kayed, R., Head, E., Thompson, J., McIntire, T., Milton, S., Cotman, C., and Glabe, C. (2003) Common Structure of Soluble Amyloid Oligomers Implies Common Mechanism of Pathogenesis. *Science (Washington, DC, U. S.) 300* (5618), 486−489.
(20) Lovell, M. A., Robertson, J. D., Teesdale, W. J., Campbell, J. L., and Markesbery, W. R. (1998) Copper, Iron and Zinc in Alzheimer's Disease Senile Plaques. *J. Neurol. Sci. 158*, 47−52.
(21) Miller, L. M., Wang, Q., Telivala, T. P., Smith, R. J., Lanzirotti, A., and Miklossy, J. (2006) Synchrotron-Based Infrared and X-Ray Imaging Shows Focalized Accumulation of Cu and Zn Co-Localized with β-Amyloid Deposits in Alzheimer's Disease. *J. Struct. Biol. 155* (1), 30−37.
(22) Bush, A. I., Pettingell, W. H., Multhaup, G., Paradis, M., Vonsattel, J., Gusella, J. F., Beyreuther, K., Masters, C. L., and Tanzi, R. E. (1994) Rapid Induction of Alzheimer Aβ Amyloid Formation by Zinc. *Science (Washington, DC, U. S.) 265* (5177), 1464−1467.
(23) Sensi, S. L., Paoletti, P., Bush, A. I., and Sekler, I. (2009) Zinc in the Physiology and Pathology of the CNS. *Nat. Rev. Neurosci. 10* (11), 780−791.
(24) Yoshiike, Y., Tanemura, K., Murayama, O., Akagi, T., Murayama, M., Sato, S., Sun, X., Tanaka, N., and Takashima, A. (2001) New Insights on How Metals Disrupt Amyloid β-Aggregation and Their Effects on Amyloid-β Cytotoxicity. *J. Biol. Chem. 276* (34), 32293−32299.
(25) Abelein, A., Gräslund, A., and Danielsson, J. (2015) Zinc as Chaperone-Mimicking Agent for Retardation of Amyloid β Peptide Fibril Formation. *Proc. Natl. Acad. Sci. U. S. A. 112* (17), 5407−5412.
(26) Lim, K. H., Kim, Y. K., and Chang, Y.-T. (2007) Investigations of the Molecular Mechanism of Metal-Induced Aβ (1−40) Amyloidogenesis. *Biochemistry 46*, 13523−13532.
(27) Miller, Y., Ma, B., and Nussinov, R. (2010) Zinc Ions Promote Alzheimer Aβ Aggregation via Population Shift of Polymorphic States. *Proc. Natl. Acad. Sci. U. S. A. 107* (21), 9490−9495.
(28) Ruggeri, F. S., Adamcik, J., Jeong, J. S., Lashuel, H. A., Mezzenga, R., and Dietler, G. (2015) Influence of the β-Sheet Content on the Mechanical Properties of Aggregates during Amyloid Fibrillization. *Angew. Chem., Int. Ed. 54* (8), 2462−2466.
(29) Khalaf, O., Fauvet, B., Oueslati, A., Dikiy, I., Mahul-Mellier, A. L., Ruggeri, F. S., Mbefo, M. K., Vercruysse, F., Dietler, G., Lee, S. J., et al. (2014) The H50Q Mutation Enhances α-Synuclein Aggregation, Secretion, and Toxicity. *J. Biol. Chem. 289* (32), 21856−21876.
(30) Glabe, C. G. (2008) Structural Classification of Toxic Amyloid Oligomers. *J. Biol. Chem. 283* (44), 29639−29643.
(31) Kayed, R., Head, E., Sarsoza, F., Saing, T., Cotman, C. W., Necula, M., Margol, L., Wu, J., Breydo, L., and Thompson, J. L. (2007) Fibril Specific, Conformation Dependent Antibodies Recognize a Generic Epitope Common to Amyloid Fibrils and Fibrillar Oligomers That Is Absent in Prefibrillar Oligomers. *Mol. Neurodegener. 2*, 1−11.
(32) Canet-Ferrer, J., Coronado, E., Forment-Aliaga, A., and Pinilla-Cienfuegos, E. (2014) Correction of the Tip Convolution Effects in the Imaging of Nanostructures Studied through Scanning Force Microscopy. *Nanotechnology 25* (39), 395703.
(33) Ha, C., Ryu, J., and Park, C. B. (2007) Metal Ions Differentially Influence the Aggregation and Deposition of Alzheimer's β-Amyloid on a Solid Template. *Biochemistry 46*, 6118−6125.
(34) Tõugu, V., Karafin, A., Zovo, K., Chung, R. S., Howells, C., West, A. K., and Palumaa, P. (2009) Zn(II)- and Cu(II)-Induced Non-Fibrillar Aggregates of Amyloid-β (1−42) Peptide Are Transformed to Amyloid Fibrils, Both Spontaneously and under the Influence of Metal Chelators. *J. Neurochem. 110*, 1784−1795.
(35) Bolognin, S., Messori, L., Drago, D., Gabbiani, C., Cendron, L., and Zatta, P. (2011) Aluminum, Copper, Iron and Zinc Differentially Alter Amyloid-Aβ1−42 Aggregation and Toxicity. *Int. J. Biochem. Cell Biol. 43* (6), 877−885.
(36) Noy, D., Solomonov, I., Sinkevich, O., Arad, T., Kjaer, K., and Sagi, I. (2008) Zinc-Amyloid β Interactions on a Millisecond Time-Scale Stabilize Non-Fibrillar Alzheimer-Related Species. *J. Am. Chem. Soc. 130* (4), 1376−1383.
(37) Castiglioni, E., Abbate, S., Longhi, G., Gangemi, R., Lauceri, R., and Purrello, R. (2007) Absorption Flattening as One Cause of Distortion of Circular Dichroism Spectra of Delta-RuPhen3 · H2TPPS Complex. *Chirality 19* (8), 642−646.
(38) Habicht, G., Haupt, C., Friedrich, R. P., Hortschansky, P., Sachse, C., Meinhardt, J., Wieligmann, K., Gellermann, G. P., Brodhun, M., Götz, J., et al. (2007) Directed Selection of a Conformational Antibody Domain That Prevents Mature Amyloid Fibril Formation by Stabilizing Aβ Protofibrils. *Proc. Natl. Acad. Sci. U. S. A. 104* (49), 19232−19237.
(39) Itkin, A., Dupres, V., Dufrêne, Y. F., Bechinger, B., Ruysschaert, J. M., and Raussens, V. (2011) Calcium Ions Promote Formation of Amyloid β-Peptide (1−40) Oligomers Causally Implicated in Neuronal Toxicity of Alzheimer's Disease. *PLoS One 6* (3), e18250.
(40) Sarroukh, R., Cerf, E., Derclaye, S., Dufrêne, Y. F., Goormaghtigh, E., Ruysschaert, J. M., and Raussens, V. (2011) Transformation of Amyloid β(1−40) Oligomers into Fibrils Is Characterized by a Major Change in Secondary Structure. *Cell. Mol. Life Sci. 68* (8), 1429−1438.
(41) Cerf, E., Sarroukh, R., Tamamizu-Kato, S., Breydo, L., Derclaye, S., Dufrêne, Y. F., Narayanaswami, V., Goormaghtigh, E., Ruysschaert, J.-M., and Raussens, V. (2009) Antiparallel β-Sheet: A Signature Structure of the Oligomeric Amyloid β-Peptide. *Biochem. J. 421* (3), 415−423.
(42) Sarroukh, R., Goormaghtigh, E., Ruysschaert, J. M., and Raussens, V. (2013) ATR-FTIR: A "Rejuvenated" Tool to Investigate Amyloid Proteins. *Biochim. Biophys. Acta, Biomembr. 1828* (10), 2328−2338.
(43) Antzutkin, O. N. (2004) Amyloidosis of Alzheimer's Aβ Peptides: Solid-State Nuclear Magnetic Resonance, Electron Paramagnetic Resonance, Transmission Electron Microscopy, Scanning Transmission Electron Microscopy and Atomic Force Microscopy Studies. *Magn. Reson. Chem. 42* (2), 231−246.
(44) Chen, S. W., Drakulic, S., Deas, E., Ouberai, M., Aprile, F. A., Arranz, R., Ness, S., Roodveldt, C., Guilliams, T., De-Genst, E. J., et al. (2015) Structural Characterization of Toxic Oligomers That Are Kinetically Trapped during α-Synuclein Fibril Formation. *Proc. Natl. Acad. Sci. U. S. A. 112* (16), E1994−E2003.
(45) Cardamone, M., and Puri, N. K. (1992) Spectrofluorimetric Assessment of the Surface Hydrophobicity of Proteins. *Biochem. J. 282* (2), 589−593.
(46) Bolognesi, B., Kumita, J. R., Pereira de Barros, T., Esbjorner, E. K., Luheshi, L. M., Crowther, D. C., Wilson, M. R., Dobson, C. M., Favrin, G., and Yerbury, J. J. (2010) ANS Binding Reveals Common Features of Cytotoxic Amyloid Species. *ACS Chem. Biol. 5* (8), 735−740.
(47) Campioni, S., Mannini, B., Zampagni, M., Pensalfini, A., Parrini, C., Evangelisti, E., Relini, A., Stefani, M., Dobson, C. M., Cecchi, C., et al. (2010) A Causative Link between the Structure of Aberrant Protein Oligomers and Their Toxicity. *Nat. Chem. Biol. 6* (2), 140−147.

DOI: 10.1021/acschemneuro.8b00141
ACS Chem. Neurosci. 2018, 9, 2959−2971

(48) Olzscha, H., Schermann, S. M., Woerner, A. C., Pinkert, S., Hecht, M. H., Tartaglia, G. G., Vendruscolo, M., Hayer-Hartl, M., Hartl, F. U., and Vabulas, R. M. (2011) Amyloid-like Aggregates Sequester Numerous Metastable Proteins with Essential Cellular Functions. *Cell 144* (1), 67−78.
(49) Mosmann, T. (1983) Rapid Colorimetric Assay for Cellular Growth and Survival: Application to Proliferation and Cytotoxicity Assays. *J. Immunol. Methods 65* (1−2), 55−63.
(50) Mannini, B., Cascella, R., Zampagni, M., van Waarde-Verhagen, M., Meehan, S., Roodveldt, C., Campioni, S., Boninsegna, M., Penco, A., Relini, A., et al. (2012) Molecular Mechanisms Used by Chaperones to Reduce the Toxicity of Aberrant Protein Oligomers. *Proc. Natl. Acad. Sci. U. S. A. 109* (31), 12479−12484.
(51) Perni, M., Galvagnion, C., Maltsev, A. S., Meisl, G., Muller, M. B. D., Challa, P. K., Kirkegaard, J. B., Flagmeier, P., Cohen, S. I. A., Cascella, R., et al. (2016) A Natural Product Inhibits the Initiation of Alpha-Synuclein Aggregation by Displacing It from Lipid Membranes and Suppresses Its Toxicity. *Proc. Natl. Acad. Sci. U. S. A. 114*, E1009.
(52) Jorgensen, E. M., and Mango, S. E. (2002) The Art and Design of Genetic Screens. *Nat. Rev. Genet. 3* (May), 356−369.
(53) Habchi, J., Chia, S., Limbocker, R., Mannini, B., Ahn, M., Perni, M., Hansson, O., Arosio, P., Kumita, J. R., Challa, P. K., et al. (2017) Systematic Development of Small Molecules to Inhibit Specific Microscopic Steps of Aβ42 Aggregation in Alzheimer's Disease. *Proc. Natl. Acad. Sci. U. S. A. 114* (2), E200−E208.
(54) Brenner, S. (1974) *Genetics of Caenorhabditis Elegans*, 71−94.
(55) Perni, M., Challa, P. K., Kirkegaard, J. B., Limbocker, R., Koopman, M., Hardenberg, M. C., Sormanni, P., Müller, T., Saar, K. L., Roode, L. W. Y., et al. (2018) Massively Parallel C. Elegans Tracking Provides Multi-Dimensional Fingerprints for Phenotypic Discovery. *J. Neurosci. Methods 306*, 57−67.
(56) Wu, J. W., Breydo, L., Isas, J. M., Lee, J., Kuznetsov, Y. G., Langen, R., and Glabe, C. (2010) Fibrillar Oligomers Nucleate the Oligomerization of Monomeric Amyloid β but Do Not Seed Fibril Formation. *J. Biol. Chem. 285* (9), 6071−6079.
(57) Breydo, L., Kurouski, D., Rasool, S., Milton, S., Wu, J. W., Uversky, V. N., Lednev, I. K., and Glabe, C. G. (2016) Structural Differences between Amyloid Beta Oligomers. *Biochem. Biophys. Res. Commun. 477* (4), 700−705.
(58) Mannini, B., Mulvihill, E., Sgromo, C., Cascella, R., Khodarahmi, R., Ramazzotti, M., Dobson, C. M., Cecchi, C., and Chiti, F. (2014) Toxicity of Protein Oligomers Is Rationalized by a Function Combining Size and Surface Hydrophobicity. *ACS Chem. Biol. 9* (10), 2309−2317.
(59) Gasteiger, E., Hoogland, C., Gattiker, A., Duvaud, S., Wilkins, M. R., Appel, R. D., and Bairoch, A. (2005) Protein Identification and Analysis Tools on the ExPASy Server. *Proteomics Protoc. Handb.*, 571−607.
(60) Uliasz, T. F., and Hewett, S. J. (2000) A Microtiter Trypan Blue Absorbance Assay for the Quantitative Determination of Excitotoxic Neuronal Injury in Cell Culture. *J. Neurosci. Methods 100* (1−2), 157−163.

DOI: 10.1021/acschemneuro.8b00141
ACS Chem. Neurosci. 2018, 9, 2959−2971